

ORIGINAL RESEARCH

Open Access



# Validation of [ $^{18}\text{F}$ ]FLT as a perfusion-independent imaging biomarker of tumour response in EGFR-mutated NSCLC patients undergoing treatment with an EGFR tyrosine kinase inhibitor

R. Iqbal<sup>1\*</sup>, G. M. Kramer<sup>1</sup>, V. Frings<sup>1</sup>, E. F. Smit<sup>2</sup>, O. S. Hoekstra<sup>1</sup>, R. Boellaard<sup>1</sup> and on behalf of the QulC-ConCePT Consortium

## Abstract

**Background:** 3'-Deoxy-3'-[ $^{18}\text{F}$ ]fluorothymidine ([ $^{18}\text{F}$ ]FLT) was proposed as an imaging biomarker for the assessment of in vivo cellular proliferation with positron emission tomography (PET). The current study aimed to validate [ $^{18}\text{F}$ ]FLT as a perfusion-independent PET tracer, by gaining insight in the intra-tumoural relationship between [ $^{18}\text{F}$ ]FLT uptake and perfusion in non-small cell lung cancer (NSCLC) patients undergoing treatment with a tyrosine kinase inhibitor (TKI). Six patients with metastatic NSCLC, having an activating epidermal growth factor receptor (EGFR) mutation, were included in this study. Patients underwent [ $^{15}\text{O}$ ]H<sub>2</sub>O and [ $^{18}\text{F}$ ]FLT PET/CT scans at three time points: before treatment and 7 and 28 days after treatment with a TKI (erlotinib or gefitinib). Parametric analyses were performed to generate quantitative 3D images of both perfusion measured with [ $^{15}\text{O}$ ]H<sub>2</sub>O and proliferation measured with [ $^{18}\text{F}$ ]FLT volume of distribution ( $V_T$ ). A multiparametric classification was performed by classifying voxels as low and high perfusion and/or low and high [ $^{18}\text{F}$ ]FLT  $V_T$  using a single global threshold for all scans and subjects. By combining these initial classifications, voxels were allocated to four categories (low perfusion-low  $V_T$ , low perfusion-high  $V_T$ , high perfusion-low  $V_T$  and high perfusion-high  $V_T$ ).

**Results:** A total of 17 perfusion and 18 [ $^{18}\text{F}$ ]FLT PET/CT scans were evaluated. The average tumour values across all lesions were  $0.53 \pm 0.26 \text{ mL cm}^{-3} \text{ min}^{-1}$  and  $4.25 \pm 1.71 \text{ mL cm}^{-3}$  for perfusion and [ $^{18}\text{F}$ ]FLT  $V_T$ , respectively. Multiparametric analysis suggested a shift in voxel distribution, particularly regarding the  $V_T$ : from an average of  $\geq 77\%$  voxels classified in the "high  $V_T$  category" to  $\geq 85\%$  voxels classified in the "low  $V_T$  category". The shift was most prominent 7 days after treatment and remained relatively similar afterwards. Changes in perfusion and its spatial distribution were minimal.

**Conclusion:** The present study suggests that [ $^{18}\text{F}$ ]FLT might be a perfusion-independent PET tracer for measuring tumour response as parametric changes in [ $^{18}\text{F}$ ]FLT uptake occurred independent from changes in perfusion.

**Trial registration:** Nederlands Trial Register (NTR), [NTR3557](https://www.trialregister.nl/trial/3557). Registered 2 August 2012

**Keywords:** Positron emission tomography (PET), Non-small cell lung cancer (NSCLC), [ $^{18}\text{F}$ ]FLT, Perfusion, Tyrosine kinase inhibitors (TKIs)

\* Correspondence: [r.iqbal@vumc.nl](mailto:r.iqbal@vumc.nl)

<sup>1</sup>Department of Radiology & Nuclear Medicine, VU University Medical Center, PO Box 7057, 1007, MB, Amsterdam, The Netherlands

Full list of author information is available at the end of the article

## Background

Non-small cell lung cancer (NSCLC) is a heterogeneous disease, comprising more than 85% of all the lung cancer cases [1]. Patients with NSCLC are often diagnosed at an advanced stage when curative treatment is no longer possible [2]. However, diagnostic advances have shown the importance of specific biological features in NSCLC, which might be used as potential therapeutic targets for treatment of these tumours [1]. One of these features includes genetic alterations of the epidermal growth factor receptor (EGFR) [3, 4].

EGFR is a transmembrane receptor with cytoplasmic kinase activity. The receptor is involved in several cellular processes such as proliferation, angiogenesis, metastasis and apoptosis [5, 6]. Patients with an activating EGFR mutation undergo continuous stimulation of the EGFR signalling pathway which results in increased proliferation, angiogenesis, metastasis and decreased apoptosis [7]. Specific targeting drugs, including tyrosine kinase inhibitors (TKIs) such as erlotinib and gefitinib, have been developed to prevent the downstream effects of the EGFR pathway [3, 8, 9].

Proliferation of (tumour) cells, one of the effects associated with the EGFR signalling pathway, can be visualised and evaluated with positron emission tomography (PET) using 3'-deoxy-3'-[<sup>18</sup>F]fluorothymidine ([<sup>18</sup>F]FLT) [3, 10–13]. Several studies have been performed to assess the correlation between [<sup>18</sup>F]FLT uptake and tumour cell proliferation as assessed with Ki-67 immunostaining. However, the results have been conflicting: while some studies confirm a positive correlation between [<sup>18</sup>F]FLT uptake and Ki-67 immunostaining [14, 15], others show a negative correlation between both. Various biological explanations, including differences in [<sup>18</sup>F]FLT metabolism, expression and activity of thymidine kinase and adenosine triphosphate levels (this is a cofactor for tyrosine kinase activity), have been proposed to explain these conflicting findings [16, 17]. Besides these, other biological features of the tumour such as its vascularity and its perfusion, might also cause variation in [<sup>18</sup>F]FLT uptake.

Perfusion is required for the delivery of nutrients, e.g. oxygen and glucose, necessary for further growth and progression of the tumour [13, 18]. Moreover, perfusion is also required for the delivery and uptake of the PET tracer in the tumour [19]. In an ideal situation, tracer delivery and tumour uptake are not perfusion dependent. However, it might be possible that perfusion affects tracer uptake: low perfused tumour lesions might show low tracer uptake due to limited supply of the tracer to the lesion. This might lead to an underestimation of the specific cellular process as assessed by the tracer; in this case, an underestimation of tumour proliferation as identified with [<sup>18</sup>F]FLT PET.

We hypothesise that [<sup>18</sup>F]FLT uptake will be decreased in low perfused tumour lesions. Furthermore, as during this study patients will be treated with a TKI, which has

an inhibiting effect on tumour angiogenesis and tumour perfusion, it can theoretically be hypothesised that during/after treatment lesions will be low vascularized and perfused. This might limit supply of the [<sup>18</sup>F]FLT tracer to the lesion, leading to decreased [<sup>18</sup>F]FLT uptake. The aim of the current study was to investigate whether [<sup>18</sup>F]FLT is a perfusion-independent PET tracer by gaining insight in the intra-tumoural relationship between [<sup>18</sup>F]FLT uptake and perfusion and their changes in EGFR mutated NSCLC patients undergoing treatment with erlotinib or gefitinib.

## Methods

### Patients

Patients ( $n = 10$ ) diagnosed with stage IV NSCLC and an activating EGFR mutation were included in this prospective clinical study. Further inclusion criteria were a primary tumour diameter of  $\geq 3$  cm and work-up for treatment with erlotinib or gefitinib. Exclusion criteria comprised pregnancy or lactation, inability to remain supine for 90 min, body weight  $> 100$  kg and metal implants (for example pacemakers). Patients were recruited at six different medical centres in The Netherlands. All scans were performed at the VU University Medical Center. The study was included in the Dutch trial register (trialregister.nl, identification number NTR3557). Prior to inclusion, each patient provided written informed consent in accordance with the regulations of the Medical Ethics Review Committee of the VU University Medical Center.

### Study rationale

Several studies have evaluated [<sup>18</sup>F]FLT as a proliferation biomarker [3, 10, 11, 14]. However, most of these studies have not taken potential perfusion effects into account [10, 11, 14]. During this study, patients will undergo treatment with a TKI, which also intervenes with the vascular endothelial growth factor (VEGF) pathway. This treatment has an inhibiting effect on tumour angiogenesis and its perfusion [20, 21]. Therefore, during this study, it might be possible to assess perfusion changes and to evaluate its effect on [<sup>18</sup>F]FLT uptake. As compared to our previous study (3) where we have investigated the relationship between [<sup>18</sup>F]FLT uptake and perfusion on whole tumour level, this study will mainly investigate the intra-tumoural relationship between both parameters.

### Data acquisition

Patients underwent [<sup>15</sup>O]H<sub>2</sub>O and [<sup>18</sup>F]FLT PET/CT scans at three different time points: before treatment and 7 and 28 days after start of treatment with a TKI (erlotinib or gefitinib). The type of TKI was chosen by the treating pulmonary physician: 150 mg of erlotinib or 250 mg of gefitinib orally once a day. In the present study, only those

patient studies were included for which all three time points were successfully acquired, i.e. at all three time points, both the [ $^{15}\text{O}$ ]H $_2$ O and [ $^{18}\text{F}$ ]FLT PET/CT scans were completed.

### Imaging protocol

The study was performed on a Gemini TF-64 PET-CT scanner (Philips Medical Systems, Cleveland, Ohio, USA). Patients had been fasting 4 h before the start of the scans to avoid possible food-induced thymidine changes. Two venous cannulae were placed, one for tracer injection and the other for blood sampling. The imaging protocol has been described in detail by Frings et al. [3]: first a 10-min dynamic [ $^{15}\text{O}$ ]H $_2$ O scan was performed after intravenous administration of 370 Mbq [ $^{15}\text{O}$ ]H $_2$ O. Next, a low-dose CT scan (50 mAs, 120 kVp) was acquired for attenuation correction of the former scan. This was followed by a 60-min [ $^{18}\text{F}$ ]FLT PET scan, after an intravenous bolus injection of 370 Mbq [ $^{18}\text{F}$ ]FLT. Afterwards, a second low-dose CT scan was obtained for attenuation correction of the [ $^{18}\text{F}$ ]FLT scan.

PET data were normalised and corrected for dead time, randoms, scatter and decay. Data were reconstructed using a vendor provided 3-dimensional row action maximum likelihood iterative reconstruction algorithm (3D RAMLA) with 3 iterations and 33 subsets, a relaxation factor of 1.0, a matrix size of  $144 \times 144$  resulting in voxel sizes of  $4 \times 4 \times 4$  mm $^3$ . These reconstructions were compliant with EANM/EARL specifications. No respiratory gating was performed. The [ $^{15}\text{O}$ ]H $_2$ O scan was reconstructed into 26 frames (1  $\times$  10, 8  $\times$  5, 4  $\times$  10, 2  $\times$  15, 3  $\times$  20, 2  $\times$  30, 6  $\times$  60 s) and the [ $^{18}\text{F}$ ]FLT scan into 36 frames (1  $\times$  10, 8  $\times$  5, 4  $\times$  10, 3  $\times$  20, 5  $\times$  30, 5  $\times$  60, 4  $\times$  150, 4  $\times$  300, 2  $\times$  600 s).

### Blood sampling

Venous blood samples were collected at 5, 10, 20, 30, 40 and 60 min post-injection. Before collecting each sample, 3–5 mL blood was drawn. This was followed by drawing a 7-mL sample and flushing of the cannula with 2.5 mL of saline afterwards. The samples were used for determining the whole-blood and plasma activity concentration and the parent fraction of [ $^{18}\text{F}$ ]FLT. These data were used to adjust an image derived (whole blood) input function to acquire a metabolite corrected plasma input function.

### Kinetic analysis

Kinetic analysis was performed using in-house developed software in Matlab (version 7.04; MathWorks Incorporation, Massachusetts, USA). For each lesion, the volume of interest (VOI) was defined on the [ $^{18}\text{F}$ ]FLT PET scan. An averaged image of the last three frames of the scan was produced and lesions

were delineated using a 50% threshold of the peak standardised uptake value ( $\text{SUV}_{\text{peak}}$ ).

Image-derived input functions (IDIFs) were generated for both [ $^{15}\text{O}$ ]H $_2$ O and [ $^{18}\text{F}$ ]FLT scans, using the early frames in which the first pass of the bolus was best visualised: VOIs of  $2 \times 2$  voxels were positioned in five consecutive axial planes within the lumen of the ascending aorta. These VOIs were then projected onto all image frames to generate a whole blood IDIF. The [ $^{18}\text{F}$ ]FLT IDIF was calibrated using the radioactivity concentrations in the venous blood samples. Moreover, IDIFs were corrected for both plasma to whole blood ratios and metabolites to obtain calibrated parent [ $^{18}\text{F}$ ]FLT plasma input functions (detailed description in Frings et al. [3]).

Next, parametric images of tumour VOIs were generated. For perfusion (tumour blood flow (TBF) =  $K_1$  of [ $^{15}\text{O}$ ]H $_2$ O), these images were generated using the basis function method [22] and for volume of distribution ( $V_T$ ) of [ $^{18}\text{F}$ ]FLT these images were generated using spectral analysis [23] with optimised settings [24]. Regionally averaged as well as voxel-by-voxel TBF and  $V_T$  data were obtained.

### Association between TBF and [ $^{18}\text{F}$ ]FLT $V_T$

The intra-tumoural association between TBF and [ $^{18}\text{F}$ ]FLT  $V_T$  was assessed on a voxel-by-voxel basis by plotting the parametric TBF values against those of [ $^{18}\text{F}$ ]FLT  $V_T$ .

### Multiparametric classification

A multiparametric classification was applied to TBF and [ $^{18}\text{F}$ ]FLT  $V_T$  data of all the lesions, using a global threshold for both parameters. The threshold was determined as the average of all tumour values of all the lesions (for all time points), for TBF and [ $^{18}\text{F}$ ]FLT  $V_T$  respectively. First of all, voxels were classified as low or high TBF and low or high  $V_T$  (independently for both parameters), using the threshold (Additional file 1: Figure S1). Voxels with values below the threshold were classified as “low TBF” or “low  $V_T$ ” whereas voxels with values above the threshold were classified as “high TBF” or “high  $V_T$ ”. This resulted in the distribution of voxels into two categories for both TBF and  $V_T$  independently (independent classification).

Next, these initial classifications were combined and voxels were classified into four categories (Additional file 1: Figure S1): lowTBF-low $V_T$ , lowTBF-high $V_T$ , highTBF-low $V_T$  and highTBF-high $V_T$  (multiparametric classification) using the method developed in Iqbal et al. [25]. Depending on the number of voxels in each category, several different voxel distribution patterns could be identified.

**Clustering index**

A quantitative metric, the clustering index (CI), was applied to describe the degree of voxel clustering (spatial grouping) within the tumour [26]. The main purpose for using this method was to gain more insight in the spatial coherence/heterogeneity of tumours and the co-localisation of voxels belonging to the same category (e.g. high FLT and high perfusion). The CI was obtained by measuring the local entropy of the classified voxels and was calculated for three (theoretical) situations to determine the expected range for CI per lesion (Additional file 1: Figure S2). By defining this range, effects of tumour volume and shape were taken into account. The following situations were simulated: (1) a condition where all voxels are classified into one category and maximally clustered within the VOI, resulting in a CI of approximately 0; (2) a condition where voxels are classified into four categories and most optimally clustered, providing a CI of approximately 0.3; (3) a condition where voxels are classified in four categories, showing random distribution and almost no clustering, resulting in a CI of approximately 2. Once the range of the CI, given by difference in CI for minimal and maximal clustering, has been determined for each lesion, the actual observed clustering can be expressed as a percentage using the following equation:

$$\text{Clustering(\%)} = \left(1 - \frac{CI_{\text{lesion}}}{CI_{\text{range}}}\right) \cdot 100 \tag{1}$$

One hundred percent clustering corresponds to the first simulated condition (maximal clustering) whereas 0% clustering corresponds to the third simulated condition (random distribution, no clustering). The CI method has been described and explained in detail by Iqbal et al. [25].

**Statistical analysis**

Statistical analyses were performed using SPSS Statistics 20 (IBM Corp.). The correlation between TBF and  $[^{18}\text{F}]\text{FLT } V_T$  (for each time point) was assessed using Pearson’s correlation coefficient. The ANOVA test was performed to assess statistical differences between tumour clustering at the three different time points.

**Results**

**Study group**

Initially, ten patients were included in this study. However, four patients did not complete imaging studies with both tracers at all time points, and therefore, these four patients were excluded from the study. Finally, the study included six patients with

stage IV NSCLC: one male and five females with an average ( $\pm$ SD) age of  $65 \pm 6$  years (Table 1). A total of six malignant lesions, all of which were primary adenocarcinomas, could be identified in the study group (Table 2). The lesions were analysed at three different time points using 17  $[^{15}\text{O}]\text{H}_2\text{O}$  and 18  $[^{18}\text{F}]\text{FLT}$  PET scans. For one patient, data of the  $[^{15}\text{O}]\text{H}_2\text{O}$  scan obtained 7 days after starting treatment was unavailable due to technical problems. Average TBF ( $\pm$ SD) values (of all lesions) at baseline and 7 and 28 days after treatment were  $0.50 \pm 0.21$ ,  $0.59 \pm 0.31$  and  $0.54 \pm 0.30$   $\text{mL cm}^{-3} \text{ min}^{-1}$ , respectively. Average  $[^{18}\text{F}]\text{FLT } V_T$  ( $\pm$ SD) values (of all lesions) at baseline and 7 and 28 days after treatment were  $5.28 \pm 1.71$ ,  $3.30 \pm 1.09$  and  $3.16 \pm 0.66$   $\text{mL cm}^{-3}$ , respectively. The average lesional values of both parameters are shown in Table 3 and Fig. 1. The global threshold (average  $\pm$  SD), as used for the multiparametric classification, were  $0.53 \pm 0.26$   $\text{mL cm}^{-3} \text{ min}^{-1}$  and  $4.25 \pm 1.71$   $\text{mL cm}^{-3}$  for TBF and  $[^{18}\text{F}]\text{FLT } V_T$  respectively.

**Association between TBF and  $[^{18}\text{F}]\text{FLT } V_T$**

The association between TBF and  $[^{18}\text{F}]\text{FLT } V_T$ , as assessed on a voxel-by-voxel basis, is represented for patient one (Fig. 2). The association was assessed at three different time points: baseline (Fig. 2a), 7 days after treatment (Fig. 2b) and 28 days after treatment (Fig. 2c). Pearson’s correlation showed no significant relationship between TBF and  $[^{18}\text{F}]\text{FLT } V_T$  (baseline,  $r = 0.14$ ,  $P = 0.79$ , 7 days after treatment,  $r = 0.24$ ,  $P = 0.69$ , 28 days after treatment,  $r = 0.41$ ,  $P = 0.43$ ). At all the three time points, data were scattered over a large range of TBF values. A specific trend, such as decreased tracer uptake with decreased TBF, could

**Table 1** Patient characteristics

All patients (n)	6
Male	1
Female	5
Age (years)	
Average	65
Range	57–75
EGFR mutation (n)	
Exon 18 G719X	2
Exon 19 Del E746-A750	1
Exon 21 L585R	3
Treatment (n)	
Erlotinib	2
Gefitinib	4

**Table 2** Lesion volumes as assessed on the [<sup>18</sup>F]FLT PET scans at the three time points: baseline, 7 days post-therapy and 28 days post-therapy

	Baseline	7 days post-therapy	28 days post-therapy
Patients	Lesion volume (mL)		
1	46.3	31.2	22.2
2	102.2	45.5	45.4
3	68.3	45.7	68.4
4	126.8	48.9	35.2
5	72.3	32.9	28.9
6	50.8	20.7	19.3

not be observed. Over the three time points, a clear decrease in [<sup>18</sup>F]FLT  $V_T$  could be perceived which was most prominent comparing the data at baseline with the data obtained 7 days after treatment. However, such a trend could not be identified for TBF.

#### Multiparametric classification

TBF and [<sup>18</sup>F]FLT  $V_T$  data were evaluated using the independent and multiparametric classification (Fig. 3). Figure 4 represents the voxel distribution patterns for one patient, for both the classifications. The overall evaluation for all patients revealed that across the three time points, changes in TBF were minimal. However, in comparison to TBF, [<sup>18</sup>F]FLT  $V_T$  underwent a shift in voxel distribution over the three time points. At baseline, most voxels were classified in the “high $V_T$ ” (average 77.1%, range 47.4–99.9%) or

**Table 3** Average TBF and [<sup>18</sup>F]FLT  $V_T$  values of all the lesions as assessed at the three time points: baseline, 7 days post-therapy and 28 days post-therapy

	Baseline	7 days post-therapy	28 days post-therapy
Patients	TBF		
1	0.46	0.40	0.44
2	0.60	0.85	0.86
3	0.47	0.58	0.39
4	0.54	0.58	0.82
5	0.32	–*	0.27
6	0.49	0.35	0.32
Patients	[ <sup>18</sup> F]FLT $V_T$		
1	5.69	3.63	3.21
2	4.89	2.75	3.30
3	7.62	2.83	3.21
4	4.75	3.71	3.20
5	5.02	4.17	3.26
6	4.20	2.70	2.54

\*TBF data for patient 5 was unavailable

“lowTBF-high $V_T$  (average 45.5%, range 14.1–70.1%) and highTBF-high $V_T$  (average 31.5%, range 2.7–59.7%)” category, depending on the classification applied (independent or multiparametric). One week after start of the therapy, most voxels were classified in the “low $V_T$ ” (average 85.4%, range 65.0–100%) or “lowTBF-low $V_T$  (average 47.7%, range (18.4–90.4%) and highTBF-low $V_T$ ” (average 41.9%, range 9.6–73.8%) category. This distribution pattern remained similar afterwards.

Visual inspection of the voxel distribution showed that voxels classified within one category were clustered. Tumours could be visually delineated into several different regions, depending on its TBF and [<sup>18</sup>F]FLT  $V_T$ . Voxels in the “lowTBF-low $V_T$ ” category were mainly located at the tumour edges whereas voxels in the “highTBF-high $V_T$ ” category could often be identified at the core of the tumour. Voxels in the remaining categories showed a more dispersed distribution pattern across the lesions.

#### Clustering index

Quantitative analysis using the CI also showed that voxels were clustered rather than randomly distributed across the lesions. It indicated that the degree of clustering was significantly different from 0% ( $P < 0.001$ ) for all three time points. Table 4 represents clustering (%) for all lesions at the three different time points (average  $\pm$  SD; baseline 59.1%  $\pm$  9.4%, 7 days post-therapy 66%  $\pm$  14.7, 28 days post-therapy 74.8%  $\pm$  4.4%). It shows an increase in clustering when comparing data at baseline with data obtained 28 days after treatment (Fig. 5; ANOVA test,  $P = 0.016$ ).

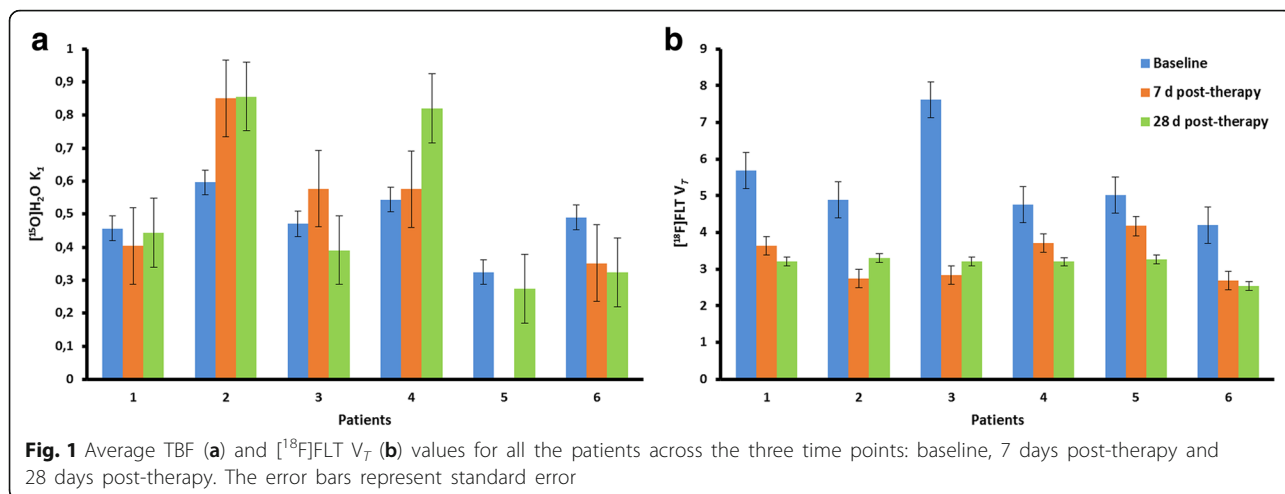
## Discussion

#### Association between TBF and [<sup>18</sup>F]FLT $V_T$

We hypothesised that TBF could affect tracer uptake: low perfused areas might show low tracer uptake due to perfusion-limited delivery of [<sup>18</sup>F]FLT. However, our data reveals that TBF does not seem to affect tracer uptake, as assessed with scatterplots (Fig. 2) and the classifications/cluster index applied. The [<sup>18</sup>F]FLT  $V_T$  is comparable in low and high perfused areas and does not correlate with TBF. In addition, changes in [<sup>18</sup>F]FLT  $V_T$  after start of treatment do not seem to accompany the (minimal) changes in TBF. This might indicate that [<sup>18</sup>F]FLT distribution and its changes do not depend on perfusion which is a preferable characteristic of the [<sup>18</sup>F]FLT PET tracer.

#### Multiparametric evaluation

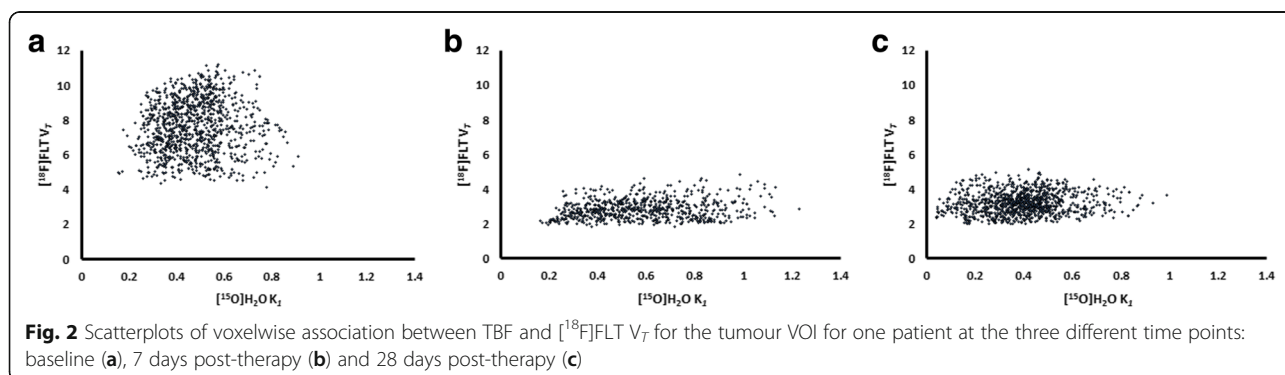
Prior to the multiparametric evaluation, TBF and [<sup>18</sup>F]FLT  $V_T$  data were evaluated independently. For TBF, most voxels were classified in the “lowTBF”

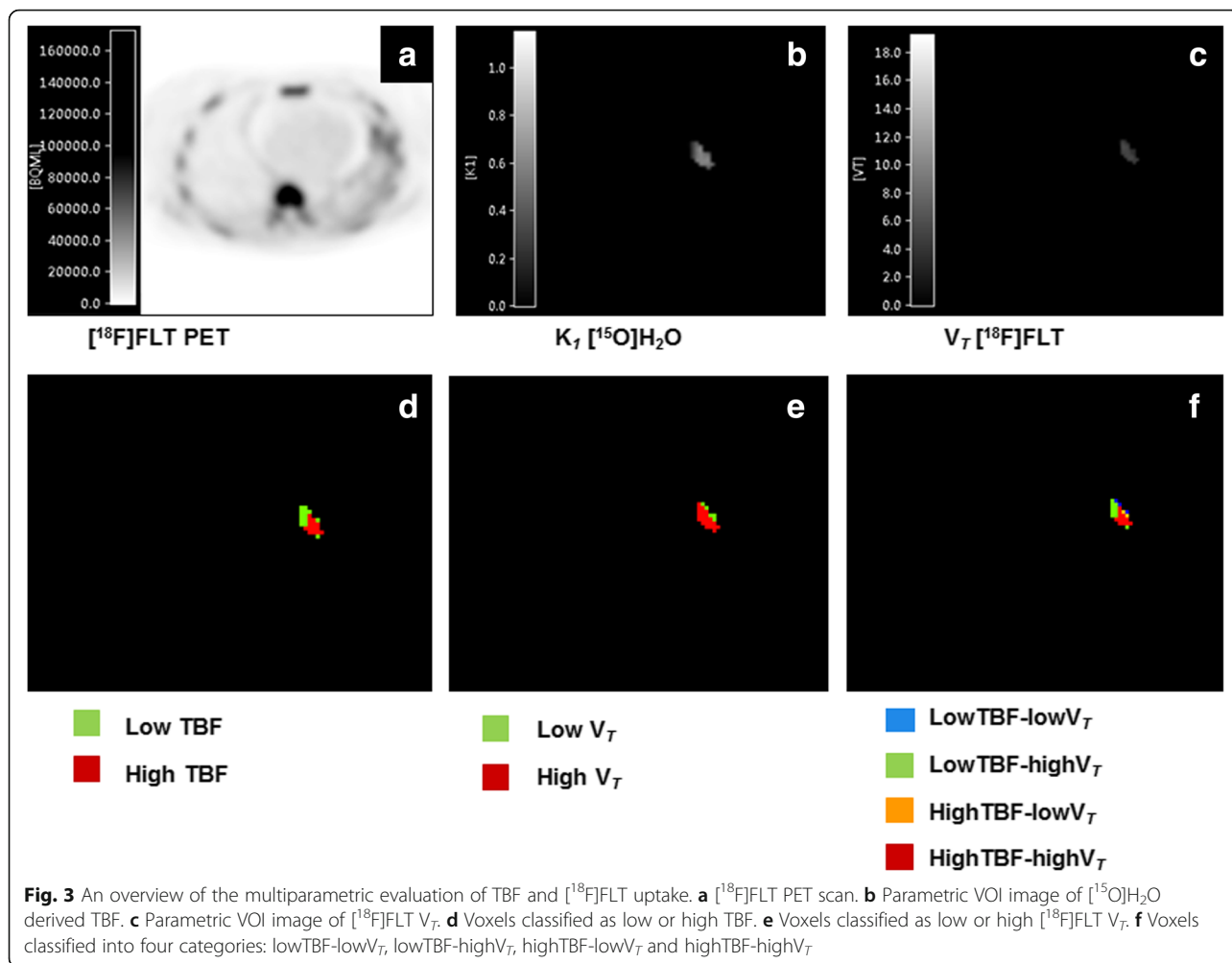


category and this distribution pattern persisted over the three time points. As patients were treated with erlotinib or gefitinib a decrease in TBF was expected. The administered TKIs influence the VEGF signalling pathway through the EGFR pathway. In healthy tissue, activation of the EGFR pathway leads to production of VEGF, the primary inducer of angiogenesis [19, 21]. However, during TKI treatment, both pathways are inhibited. This results in decreased angiogenesis, eventually resulting in decreased TBF and tumour necrosis. De Langen et al. monitored response to antiangiogenic therapy (bevacuzimab and erlotinib) by investigating changes in TBF [9]. They assessed that mean TBF decreased by 11% 3 weeks after starting treatment. Another study also showed a decrease in TBF 2 weeks after treatment with Sunitinib [27]. Mankhoff et al. investigated changes in TBF in patients receiving neoadjuvant chemotherapy [28]. They differentiated between responders and non-responders, the first showing a decrease in TBF whereas the latter showed an increase in TBF. Although our study does not show distinct changes in TBF, it might be possible that these changes occur at a later stage of treatment as angiogenesis and perfusion changes are relatively slow processes.

Furthermore, our data shows that  $[^{18}\text{F}]\text{FLT } V_T$  decreases after start of TKI treatment with the most prominent decrease observed 7 days after treatment. Kahraman et al. also presented similar results in NSCLC patients, showing decreased  $[^{18}\text{F}]\text{FLT}$  uptake in early PET images (1 week after starting treatment with erlotinib) [29]. They concluded that early evaluation with  $[^{18}\text{F}]\text{FLT}$  PET is better than late evaluation (6 weeks after treatment with erlotinib) for response prediction and prediction of progression-free survival. Several other studies also showed a decrease in  $[^{18}\text{F}]\text{FLT}$  uptake 1 or 2 weeks after therapy, which correlated with progression-free survival [12, 30]. Our study also evaluated survival data to assess a possible relationship between overall survival and the voxel distribution patterns of the multiparametric classification. However, no such relationship could be found, possibly due to the small population size.

In addition, the visual analysis suggested that voxels classified within one category were clustered rather than randomly distributed across the lesions. It was possible to visually delineate a tumour into several different regions, depending on the voxel distribution of TBF and  $[^{18}\text{F}]\text{FLT } V_T$  independently and multiparametric. Voxels in the



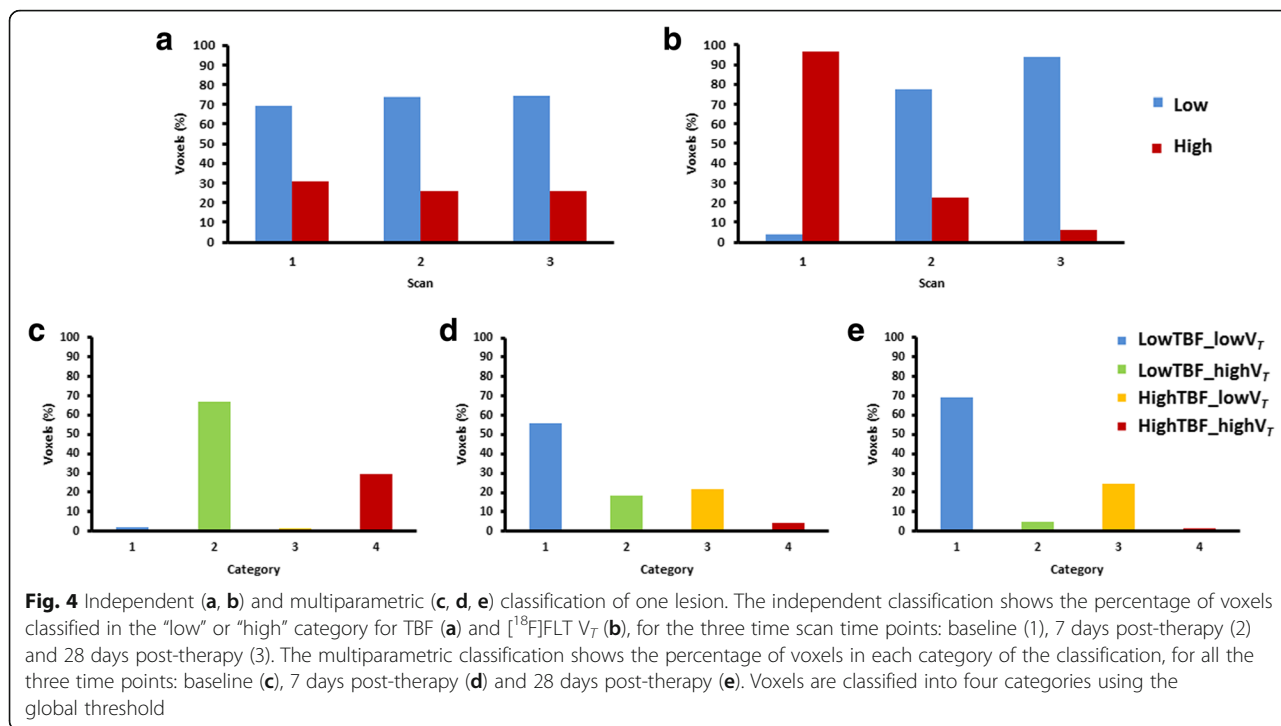


“lowTBF-low $V_T$ ” category were mainly located at the tumour edges; this might be a partial volume effect: due to tumour movement caused by respiration, the PET signal might be blurred, therefore showing a low PET signal [25]. On the contrary, voxels in the “highTBF-high $V_T$ ” category could often be identified at the core of the tumour, indicating high angiogenesis and proliferation in the core of the tumour [25]. The voxel distribution varied intralesionally as well as interlesionally, indicating spatial heterogeneity of these tumours [31, 32]. This can be the result of heterogeneity at genetic and cellular levels as well as at a tissue level [33–35]. The first refers to mutational events, which take place during tumour development. These mutations might vary between tumours, which might be one of the mechanisms responsible for differences in response to treatment and resistance to treatment. The heterogeneity at the tissue level indicates differences in vascular density, blood flow, regional metabolism and proliferation. This study assessed the diversity of TBF and

proliferation rate within NSCLC tumours and showed that each tumour has its own heterogeneity.

### Limitations and scientific implications

This study has certain limitations, and one of these includes the small sample size ( $n=6$ , with each three scans). To increase the reliability of the study performed, it would be recommended to perform it with a larger sample size in future. Secondly, as during this study patients with lung cancer were scanned (scanning field: thorax), respiratory motion might have led to imaging artefacts (this might have affected further analysis and the results) or reduced spatial resolution. However, the presence of respiratory motion-related artefacts was carefully checked and these were not visually identified. Moreover, the primary tumours in our study were relatively large ( $\geq 3$  cm diameter), and for these tumours, the tracer uptake is usually less affected by motion. Yet, to limit the presence of respiratory motion artefacts, respiratory gating might be a helpful technique for future studies. Finally, while



performing the kinetic analysis, lesions on PET scans were delineated using the 50%  $\text{SUV}_{\text{peak}}$  threshold. This might have led to exclusion of low perfused and/or low tracer uptake areas. However, during our study, visual inspection of the VOI using both PET and CT data did not suggest that tumour tissue was missed and this threshold could be used.

In our study, we evaluated the relationship of tumour perfusion and  $[^{18}\text{F}]\text{FLT}$  tracer uptake responses in patients suffering from adenocarcinoma and treated with EGFR TKIs. We found that  $[^{18}\text{F}]\text{FLT}$  responses occurred independent from perfusion (changes), which suggests that  $[^{18}\text{F}]\text{FLT}$  uptake and its change may be considered as a unique biomarker

**Table 4** Clustering (%) represents the degree of voxel clustering for all lesions, for the three time points: baseline, 7 days post-therapy and 28 days post-therapy. Voxels are more clustered when the percentage is closer to 100%

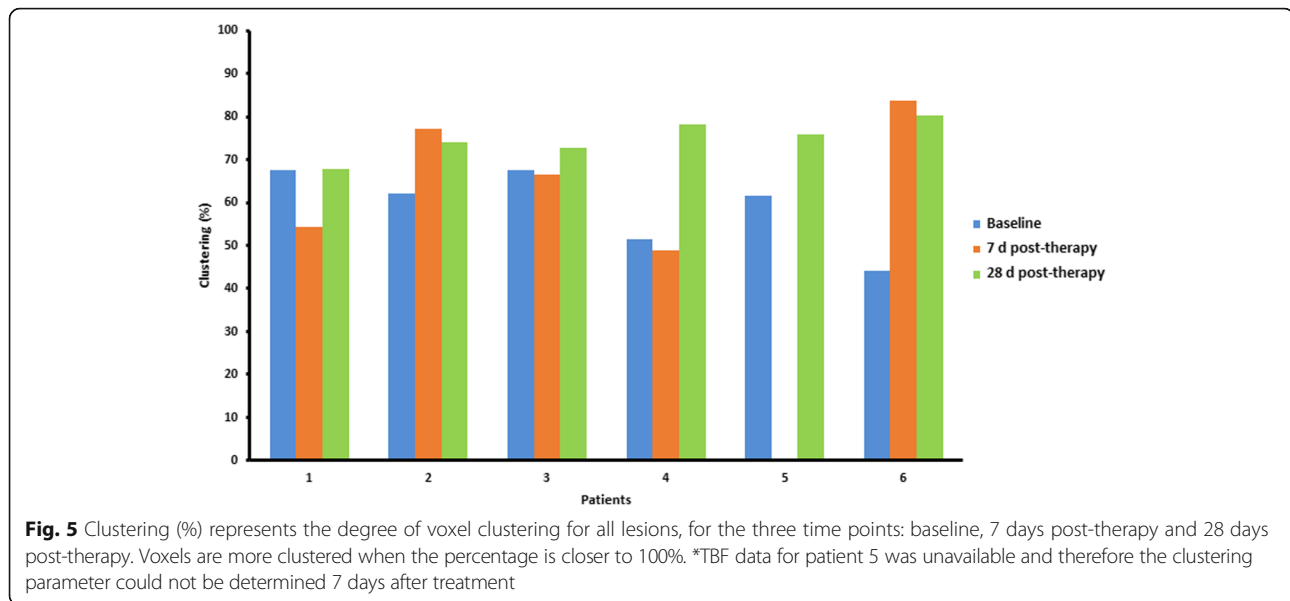
Patients	Clustering (%)		
	Baseline	7 days post-therapy	28 days post-therapy
1	67.8	54.3	67.8
2	62.1	77.1	73.9
3	67.4	66.7	72.7
4	51.5	49.0	78.2
5	61.6	—*	75.8
6	44.2	83.8	80.3

\*TBF data for patient 5 was unavailable and therefore the clustering parameter could not be determined

independent from perfusion. The authors believe that these results are generally applicable to other types of NSCLC patients and therapies. However, for other patients and therapies, a treatment response or change in both perfusion and  $[^{18}\text{F}]\text{FLT}$  uptake might occur. Our results, however, suggest that  $[^{18}\text{F}]\text{FLT}$  uptake changes as a response marker can be observed regardless of change in perfusion.

$[^{15}\text{O}]\text{H}_2\text{O}$  and  $[^{18}\text{F}]\text{FLT}$  PET are a non-invasive method for the assessment of perfusion and cellular proliferation, respectively. The acquired data was used for generating the multiparametric classification. As it is a new method for analysing changes in perfusion and tracer uptake, further evaluation of this method is necessary to reliably apply this in future studies. Clinical data, such as resection specimens, could be useful for the assessment of perfusion and proliferation (using immunohistochemical staining). It would be interesting to compare pathology with the results of the multiparametric classification and investigate similarities or differences. It would also be interesting to assess perfusion and proliferation at a later stage of treatment. During the follow-up of this study, changes in perfusion were limited, while changes in proliferation were prominent. It might be interesting to see how this evolves when patients are under treatment for a longer time as in that case changes in perfusion might occur or become more prominent as angiogenesis and perfusion changes are relatively slow processes.





## Conclusion

The present study suggests that [ $^{18}\text{F}$ ]FLT might be a perfusion-independent PET tracer for measuring tumour response as parametric changes in [ $^{18}\text{F}$ ]FLT uptake occurred independent from changes in perfusion.

## Additional file

**Additional file 1: Figure S1.** A representation of different voxel distribution patterns. The presented distributions are hypothetical. The independent classification consists of voxels classified in two categories, low and high, for TBF and [ $^{18}\text{F}$ ]FLT  $V_T$  independently (independent classification). A combination of these classifications results in the multiparametric classification, where voxels are classified into four categories: lowTBF-low $V_T$  (category 1), lowTBF-high $V_T$  (category 2), highTBF-low $V_T$  (category 3), highTBF-high $V_T$  (category 4). **Figure S2.** A representation of three possible patterns of voxel clustering. (a) Pattern which represents maximal clustering. (b) Pattern which represents optimal clustering with voxels classified in four different categories. (c) Pattern which represents random distribution of voxels classified in four different categories. (DOC 215 kb)

## Abbreviations

[ $^{18}\text{F}$ ]FLT: 3'-Deoxy-3'-[ $^{18}\text{F}$ ]fluorothymidine; 3D RAMLA: 3-Dimensional row action maximum likelihood reconstruction algorithm; CI: Clustering index; EGFR: Epidermal growth factor receptor; IDIF: Image-derived input function; NSCLC: Non-small cell lung cancer; PET: Positron emission tomography; SUV<sub>peak</sub>: Peak standardised uptake value; TBF: Tumour blood flow; TKI: Tyrosine kinase inhibitor; VEGF: Vascular endothelial growth factor; VOI: Volume of interest;  $V_T$ : Volume of distribution

## Acknowledgements

The authors would like to thank the patients for participating in this study. We would also like to thank the members of the Department of Radiology & Nuclear Medicine of the VU University Medical Center for tracer production and data acquisition. The study has been performed within the framework of the QuIC-ConCePT Consortium, whose participants include AstraZeneca, the European Organisation for Research and Treatment of Cancer (EORTC), Cancer Research U.K., the University of Manchester, Westfälische Wilhelms-Universität Münster, Radboud University Nijmegen Medical Center, Institut National de la Santé et de la Recherche Médicale, Stichting Maastricht Radiation Oncology

"Maastric Clinic," VUmc Amsterdam, King's College London, Universitair Ziekenhuis Antwerpen, Institute of Cancer Research–Royal Cancer Hospital, Erasmus Universitair Medisch Centrum Rotterdam, Imperial College of Science Technology and Medicine, Keosys S.A.S., Eidgenössische Technische Hochschule Zürich, Amgen NV, Eli Lilly and Company Ltd., GlaxoSmithKline Research & Development Limited, Merck KGa, Pfizer Limited, F. Hoffmann–La Roche Ltd., and Sanofi-Aventis Research and Development.

## Funding

This research has received support from the Innovative Medicines Initiative Joint Undertaking (<http://www.imi.europa.eu>; grant agreement no. 115151), whose resources are composed of a financial contribution from the European Union's Seventh Framework Programme (FP7/2007-2013) and an in-kind contribution from the companies of the European Federation of Pharmaceutical Industries and Associations. We also acknowledge the Quantitative Imaging in Cancer: Connecting Cellular Processes with Therapy project (QuIC-ConCePT project) from the Innovative Medicines Initiative (IMI) for partly funding the project. No other potential conflicts of interest relevant to this article were reported.

## Availability of data and materials

The data supporting the conclusions of this article is included within the article.

## Authors' contributions

RI contributed to the concept, design, data-analysis and interpretation, drafting and revision of the manuscript. GMK contributed to the data acquisition and analysis, critical review and revision of the manuscript. VF contributed to the data acquisition and analysis, critical review and revision of the manuscript. EFS contributed to the design, critical review and revision of the manuscript. OSH contributed to the concept, design, critical review and revision of the manuscript. RB contributed to the concept, design, data-analysis and interpretation, drafting and revision of the manuscript. All authors read and approved the final manuscript

## Ethics approval and consent to participate

This study has been performed in accordance with the Declaration of Helsinki, and it has been approved by the Medical Ethics Review Committee of the VU University Medical Center. Informed consent was obtained from all individual participants included in the study.

## Consent for publication

All participants included in this study provided consent for publication.

**Competing interests**

The authors declare that they have no competing interests.

**Publisher's Note**

Springer Nature remains neutral with regard to jurisdictional claims in published maps and institutional affiliations.

**Author details**

<sup>1</sup>Department of Radiology & Nuclear Medicine, VU University Medical Center, PO Box 7057, 1007, MB, Amsterdam, The Netherlands. <sup>2</sup>Department of Pulmonology, VU University Medical Center, Amsterdam, The Netherlands.

Received: 6 December 2017 Accepted: 15 March 2018

Published online: 27 March 2018

**References**

- Chen Z, Fillmore CM, Hammerman PS, Kim CF, Wong K. Non-small-cell lung cancers: a heterogeneous set of diseases. *Nat Rev Cancer*. 2014;14:535–46.
- Thunnissen E, Smit EF, Nederland PM, Dingemans AC. EGFR-mutatie bij niet-kleincellig longcarcinoom. *Ned Tijdschr Geneesk*. 2011;155:A2554.
- Frings V, Yaqub M, Hoynq LL, et al. Assessment of simplified methods to measure 18F-FLT uptake changes in EGFR-mutated non-small cell lung cancer patients undergoing EGFR tyrosine kinase inhibitor treatment. *J Nucl Med*. 2014;55:1417–23.
- Lynch TJ, Bell DW, Sordella R, et al. Activating mutations in the epidermal growth factor receptor underlying responsiveness of non-small-cell lung cancer to gefitinib. *N Engl J Med*. 2004;350:2129–39.
- Ranson M. Epidermal growth factor receptor tyrosine kinase inhibitors. *Br J Cancer*. 2004;90:2250–5.
- Arora A, Scholar EM. Role of tyrosine kinase inhibitors in cancer therapy. *J Pharmacol Exp Ther*. 2005;315:971–9.
- Gazdar AF. Activating and resistance mutations of EGFR in non-small-cell lung cancer: role in clinical response to EGFR tyrosine kinase inhibitors. *Oncogene*. 2009;28:S24–31.
- Da Cunha SG, Shepherd FA, Tsao MS. EGFR mutations and lung cancer. *Annu Rev Pathol*. 2011;6:49–69.
- De Langen AJ, Van den Boogaart V, Lubberink M, et al. Monitoring response to antiangiogenic therapy in non-small cell lung cancer using imaging markers derived from PET and dynamic contrast-enhanced MRI. *J Nucl Med*. 2011;52:48–55.
- Salskov A, Tammisetti VS, Grierson J, Vesselle H. FLT: measuring tumor cell proliferation in vivo with positron emission tomography and 3'-deoxy-3'-[18F]fluorothymidine. *Semin Nucl Med*. 2007;37:429–39.
- Chen XT, Zhao X, Gao ZH, et al. Proliferation PET image to characterize pathological spatial features in patients with non-small cell lung cancer: a pilot study. *Int J Clin Exp Med*. 2015;8:9758–64.
- Bollineni VR, Kramer GM, Jansma EP, Liu Y, Oyen WJ. A systematic review on [(18)F]FLT-PET uptake as a measure of treatment response in cancer patients. *Eur J Cancer*. 2016;55:81–97.
- Yang W, Zhang Y, Fu Z, Sun X, Mu D, Yu J. Imaging proliferation of 18F-FLT PET/CT correlated with the expression of microvessel density of tumour tissue in non-small-cell lung cancer. *Eur J Nucl Med Mol Imaging*. 2012;39:1289–96.
- Vesselle H, Grierson J, Muzi M, et al. In vivo validation of 3'-deoxy-3'-[(18)F]fluorothymidine ((18F)FLT) as a proliferation imaging tracer in humans: correlation of [(18F)FLT] by positron emission tomography with Ki-67 immunohistochemistry and flow cytometry in human lung tumors. *Clin Cancer Res*. 2002;8:3315–23.
- Chalkidou A, Landau DB, Odell EW, Cornelius VR, O'Doherty MJ, Marsden PK. Correlation between Ki-67 immunohistochemistry and 18F-fluorothymidine uptake in patients with cancer: a systematic review and meta-analysis. *Eur J Cancer*. 2012;48:3499–513.
- McKinley ET, Ayers GD, Smith RA, Saleh SA, Zhao P, Washington MK, et al. Limits of [18F]-FLT PET as biomarker of proliferation in oncology. *PLoS One*. 2013;8:e58938.
- Schelhaas S, Heinzmann K, Bollineni VR, et al. Preclinical applications of 3'-deoxy-3'-[18F]fluorothymidine in oncology—a systematic review. *Theranostics*. 2017;7:40–50.
- Verwer EE, Boellaard R, Van der Veldt AM. Positron emission tomography to assess hypoxia and perfusion in lung cancer. *World J Clin Oncol*. 2014;5:824–44.
- Bogin L, Margalit R, Mispelter J, Degani H. Parametric imaging of tumor perfusion using flow- and permeability-limited tracers. *J Magn Reson Imaging*. 2002;16:289–99.
- O'Byrne KJ, Koukourakis MI, Giatromanolaki A, et al. Vascular endothelial growth factor, platelet-derived endothelial cell growth factor and angiogenesis in non-small-cell lung cancer. *Br J Cancer*. 2000;82:1427–32.
- Kerbel RS. Tumor angiogenesis. *N Engl J Med*. 2008;358:2039–49.
- Boellaard R, Knaapen P, Rijbroek A, Luurtsema GJJ, Lammertsma AA. Evaluation of basis function and linear least squares methods for generating parametric blood flow images using 15O-water and positron emission tomography. *Mol Imaging Biol*. 2005;7:273–85.
- Cunningham VJ, Jones T. Spectral analysis of dynamic PET studies. *J Cereb Blood Flow Metab*. 1993;13:15–23.
- Kramer GM, Frings V, Heijtel D, Smit EF, Hoekstra OS, Boellaard R. Parametric method performance for dynamic 18F-FLT PET/CT in EGFR-mutated NSCLC patients prior and during therapy. *J Nucl Med*. 2017;58:920–5.
- Iqbal R, Kramer GM, Verwer EE, Huisman MC, De Langen AJ, Bahce I, et al. Multiparametric analysis of the relationship between tumor hypoxia and perfusion using 18F-FAZA and 15O-H2O PET. *J Nucl Med*. 2015;57:530–5.
- Tixier F, Rest CCL, Hatt M, et al. Intratumor heterogeneity characterized by textural features on baseline 18F-FDG PET images predicts response to concomitant radiochemotherapy in esophageal cancer. *J Nucl Med*. 2011;52:369–78.
- Scott AM, Mitchell PL, O'Keefe G, et al. Pharmacodynamic analysis of tumour perfusion assessed by 15O-water PET imaging during treatment with sunitinib malate in patients with advanced malignancies. *EJNMMI Res*. 2012;2:31.
- Mankoff DA, Dunnwald LK, Gralow JR, et al. Changes in blood flow and metabolism in locally advanced breast cancer treated with neoadjuvant chemotherapy. *J Nucl Med*. 2003;44:1806–18014.
- Kahraman D, Scheffler M, Zander T, et al. Quantitative analysis of response to treatment with erlotinib in advanced non-small cell lung cancer using 18F-FDG and 3'-deoxy-3'-[18F]fluorothymidine PET. *J Nucl Med*. 2011;52:1871–7.
- Kenny L, Coombes RC, Viquishin DM, Al-Nahhas A, Shousha S, Aboagye EO. Imaging early changes in proliferation at 1 week post chemotherapy: a pilot study in breast cancer patients with 3'-deoxy-3'-[18F]fluorothymidine positron emission tomography. *Eur J Nucl Med Mol Imaging*. 2007;34:1339–47.
- Laymon CM, Oborski MJ, Lee VK, et al. Combined imaging biomarkers for therapy evaluation in glioblastoma multiforme: correlating sodium MRI and F-18 FLT PET on a voxel-wise basis. *Magn Reson Imaging*. 2012;30:1268–78.
- Veronese M, Rizzo G, Aboagye EO, Bertoldo A. Parametric imaging of 18F-fluoro-3-deoxy-3-L-fluorothymidine PET data to investigate tumour heterogeneity. *Eur J Nucl Med Mol Imaging*. 2014;41:1781–92.
- Willaime JM, Turkheimer FE, Kenny LM, Aboagye EO. Quantification of intra-tumour cell proliferation heterogeneity using imaging descriptors of 18F-fluorothymidine-positron emission tomography. *Phys Med Biol*. 2013;58:187–203.
- Marusyk A, Polyak K. Tumor heterogeneity: causes and consequences. *Biochim Biophys Acta*. 1805;2010:105–17.
- Basu S, Kwee TC, Gatenby R, Saboury B, Torigian DA, Alavi A. Evolving role of molecular imaging with PET in detecting and characterizing heterogeneity of cancer tissue at the primary and metastatic sites, a plausible explanation for failed attempts to cure malignant disorders. *Eur J Nucl Med Mol Imaging*. 2011;38:987–91.

**Submit your manuscript to a SpringerOpen® journal and benefit from:**

- Convenient online submission
- Rigorous peer review
- Open access: articles freely available online
- High visibility within the field
- Retaining the copyright to your article

Submit your next manuscript at ► [springeropen.com](http://springeropen.com)